

Morphological Characterization of a Low-Bandgap Crystalline Polymer:PCBM Bulk Heterojunction Solar Cells

Haiyun Lu, Bulent Akgun, and Thomas P. Russell*

Understanding the morphology of polymer-based bulk heterojunction (BHJ) solar cells is necessary to improve device efficiencies. Blends of a low-bandgap silole-containing conjugated polymer, poly[(4,4'-bis(2-ethylhexyl)dithieno[3,2-b;2',3'-d]silole)-2,6-diyl-alt-(4,7-bis(2-thienyl)-2,1,3-benzothiadiazole)-5,5'-diyl] (PSBTBT) with [6,6]phenyl-C₆₁-butyric acid methyl ester (PCBM) were investigated under different processing conditions. The surface morphologies and vertical segregation of the "As-Spun", "Pre-Annealed", and "Post-Annealed" films were studied by scanning force microscopy, contact angle measurements, X-ray photoelectron spectroscopy, near-edge X-ray absorption fine structure spectroscopy, dynamic secondary ion mass spectrometry, and neutron reflectivity. The results showed that PSBTBT was enriched at the cathode interface in the "As-Spun" films and thermal annealing increased the segregation of PSBTBT to the free surface, while thermal annealing after deposition of the cathode increased the PCBM concentration at the cathode interface. Grazing-incidence X-ray diffraction and small-angle neutron scattering showed that the crystallization of PSBTBT and segregation of PCBM occurred during spin coating, and thermal annealing increased the ordering of PSBTBT and enhanced the segregation of the PCBM, forming domains ~10 nm in size, leading to an improvement in photovoltaic performance.

1. Introduction

Bulk heterojunction (BHJ) organic photovoltaic (OPV) systems have attracted increasing interest due to their low-cost and potential for highly scalable solution processing. However, achieving efficiencies in excess of 10% is an important milestone in making OPV devices viable economically. While

there have been advances in the synthesis of novel low bandgap polymers and block copolymers with tailored morphologies, translating these advances to large scale production mandates understanding the morphology of the active layer developed during processing, the relationship of the morphology to device performance, and routes to tailor the morphology to optimize efficiency.^[1-4] Controlling the morphology is made even more challenging, since the morphology of the active layer is far-removed from equilibrium, resulting from a competition between the ordering of the photoactive polymer, the phase separation of the components, the rate of solvent evaporation, and the mobility and interfacial segregation of the components.^[5,6]

The most-studied donor-acceptor combination for polymer solar cells is a blend of poly(3-hexylthiophene) (P3HT) and [6,6]phenyl-C₆₁-butyric acid methyl ester (PCBM), solution cast from 1,2-dichlorobenzene (*o*-DCB), where subsequent thermal annealing at temperatures well below the melting point of P3HT significantly improves device performance.^[7] The improved performance has been attributed to an improvement in the molecular ordering of P3HT within nanoscopic domains in the active layer,^[8,9] enhanced separation of the components leading to phase purity, and preferential segregation of components to the anode and cathode interfaces.^[10] Scanning probe microscopy (SPM) techniques, including scanning force and Kelvin-force microscopies,^[11-13] near-edge X-ray absorption fine structure analysis (NEXAFS)^[10,14,15] have been used to study the surface structure and morphology of the active layer. Synchrotron-based hard X-ray techniques, including grazing incidence X-ray diffraction (GIXD),^[8,9,16-19] grazing incidence small angle X-ray scattering,^[20] resonance soft X-ray scattering (RSOXS),^[21] NEXAFS analysis,^[10,14,15] and scanning transmission X-ray spectromicroscopy^[22] have been used to characterize the ordering, orientation and phase behavior of the components near the surface and within the interior of the active layer.

The spatial distribution of the components normal to the film surface and the segregation of the components at the electrode interfaces in BHJ blend films is crucial to the charge generation and transport processes, and has received increasing attention, since the first report on vertical segregation in a

Dr. H. Lu, Prof. T. P. Russell
Department of Polymer Science and Engineering
University of Massachusetts
Amherst, Massachusetts 01003, USA
E-mail: russell@mail.pse.umass.edu

Dr. B. Akgun
NIST Center for Neutron Research
National Institute of Standards and Technology (NIST)
Gaithersburg, Maryland 20899, USA

Dr. B. Akgun
Department of Material Science and Engineering
University of Maryland
College Park, Maryland 20742, USA

DOI: 10.1002/aenm.201100128

semiconductor blend film of poly(9,9'-dioctylfluorene-co-bis-N,N'-(4-butylphenyl)-bis-N,N'-phenyl-1,4-phenylenediamine) and poly(9,9'-dioctylfluorene-co-benzothiadiazole) studied by SPM.^[23] Through the use of variable-angle spectroscopic ellipsometry, Campoy-Quiles and co-workers obtained the vertical composition profiles of P3HT/PCBM blends on a hydrophilic substrate, where the as-cast film showed an enrichment of PCBM and P3HT at the film/substrate and film/air interfaces, respectively, and thermal or solvent vapor annealing increased the segregation.^[24] On the basis of a lift-off sample preparation and X-ray photoelectron spectroscopy (XPS), Yang and co-workers also reported the vertical phase separation in P3HT/PCBM BHJs.^[25] Recently, low-impact energy secondary ion mass spectrometry has been used to study the polymer-metal interface and the composition profiles normal to the film surface in P3HT/PCBM BHJ devices, where large gradients in the composition of P3HT and PCBM were found within the active layer, with a cathode/BHJ interface that was enriched in P3HT.^[26]

Due to the large natural contrast between PCBM and semiconductor polymers like P3HT, neutron reflectivity (NR), with a spatial resolution of a nanometer or less, has been used to characterize the vertical distribution of PCBM in the BHJ active layers.^[27–29] PCBM was found to concentrate at the substrate interface and near but not at the air interface where the aluminum counter-electrode was deposited.

While many techniques are now being used to probe the structure and morphology of the active layer in OPVs, the highly non-equilibrium nature of the morphology, the complexities introduced by solvent evaporation in the development of the morphology, and differences in the characteristics of the P3HTs used in the different studies have given rise to inconsistencies in the description of the structure and morphology in OPV active layers. In addition, the structure of the active layer adjacent to the electrode interfaces can be markedly different from that found in the interior of the active layer and will also be strongly dependent upon whether thermal annealing is done prior to (“Pre-Annealed”) or after (“Post-Annealed”) the deposition of electrodes. Only a few studies on morphological characterization of the annealed devices were performed in the presence of an Al electrode.^[26,30–32] It has been found that thermal annealing in the presence of an Al electrode reduces the preferred orientation of P3HT and Al diffuses into the organic films to form intermediate thin gradient layer.^[30–32] By removing Al electrode after post-annealing, Ohkita and co-workers^[33] and Chen et al.^[32] measured the surface composition of the P3HT/PCBM solar cell blends by XPS and NEXAFS, demonstrating a surface segregation of PCBM at the cathode/active layer interface induced by post-annealing.

In this work, we systematically investigated the morphology of blends of PCBM with a silole-containing low-bandgap polymer, poly[(4,4'-bis(2-ethylhexyl)dithieno[3,2-b:2',3'-d]silole)-2,6-diyl-alt-(4,7-bis(2-thienyl)-2,1,3-benzothiadiazole)-5,5'-diyl] (PSBTBT). It has been shown that this polymer is highly crystalline and has improved charge transport properties, reduced bimolecular recombination, and a reduced formation of charge transfer complexes when blended with a fullerene derivative.^[34–37] The solar cells based on blends of PSBTBT and [6,6] phenyl-C71-butyric acid methyl ester (C₇₀-PCBM) prepared

by doctor blading have efficiencies of 5.2%.^[38] Processed with chloroform instead of *o*-DCB, an efficiency of 5.6% was achieved with the same materials by Yang and co-workers.^[37] Other silole-containing low-bandgap polymers, like poly[(4,4-didodecyldithieno[3,2-b:2',3'-d]silole)-2,6-diyl-alt-(2,1,3-benzothiadiazole)-4,7-diyl] (Si-PDTBT) also showed promising solar cell performances.^[39]

Here, PSBTBT and its blends with PCBM were used as models for understanding the active layer in OPV devices based on low-bandgap conjugated polymers under different processing conditions. To provide insight into the performance of these mixtures in actual devices, experiments were performed on thin films on substrates coated with a layer of poly(ethylenedioxythiophene):polystyrene sulfonate (PEDOT:PSS). Thermal annealing was done prior to (“Pre-Annealing”) and after (“Post-Annealing”) the deposition of Al cathodes, mimicking the real solar cell structures. The surface morphologies, compositions, and molecular orientation of the “As-Cast”, “Pre-Annealed”, and “Post-Annealed” thin films were studied with scanning force microscopy (SFM), contact angle measurements, X-ray photoelectron spectroscopy (XPS), and near edge X-ray absorption fine structure (NEXAFS) spectroscopy. The vertical segregation of the blend films was investigated by dynamic secondary ion mass spectrometry (DSIMS) and neutron reflectivity (NR). In addition, grazing incidence X-ray diffraction (GIXD) was used to study the ordering of the PSBTBT in the films under different treatments. Small angle neutron scattering (SANS) was used to investigate the uniformity in the distribution and degree of mixing between the two components in the plane of the film. The diffusion of PCBM in PCBM/PSBTBT bilayer films was studied by NR and DSIMS.

2. Results and Discussion

2.1. Device Performance

The bandgap and the highest occupied molecular orbital (HOMO) energy levels of PSBTBT and PCBM were measured by UV-vis absorption and ultraviolet photoelectron spectroscopy, from which the energy diagram was determined (see Supporting Information Figure S1). The configuration of the photovoltaic device based on PSBTBT:PCBM blends is schematically shown in **Figure 1A**. **Figure 1B** shows the representative current density–voltage (J – V) curves for the “As-Cast”, “Post-Annealed” and “Pre-Annealed” devices under dark and AM1.5G illumination. The “Post-Annealed” device did not show an obvious change in open-circuit voltage (V_{OC}) but did increase the short-circuit current (J_{SC}) and improve the fill factor (FF). However, after “Pre-Annealing”, both the V_{OC} and FF of the device were decreased, and the power conversion efficiency (PCE) decreased by 18% in comparison to the “As-Cast” devices. **Table 1** lists some of the photovoltaic characterization data for the “As-Cast” devices and devices “Post-Annealed” at 150 °C for different times. A brief annealing at 150 °C improved the J_{SC} and FF, and consequently, the PCE. The PCE reached a maximum when the device was “Post-Annealed” at 150 °C for 1 min. With further annealing the J_{SC} , FF and PCE dropped significantly. After 20 minutes of annealing, the PCE was even lower than that of the “As-Cast”.

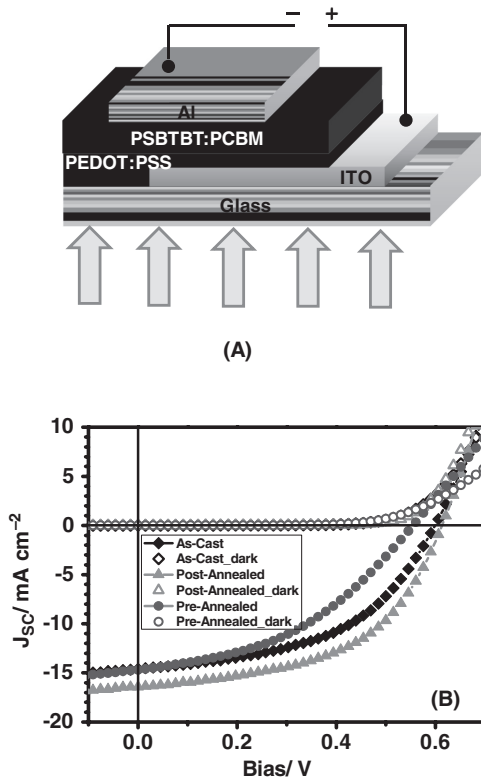


Figure 1. (A) Schematic of the PSBTBT:PCBM-based solar cell devices. (B) The current density–voltage curves of the “As-Cast”, “Pre-Annealed”, and “Post-Annealed” PSBTBT:PCBM solar cells at dark (open symbols) and under AM 1.5G irradiation (filled symbols). The annealing condition for both the “Pre-Annealed” and “Post-Annealed” samples is at 150 °C for 1 min.

The photovoltaic performance of the devices at other “Post-Annealing” temperatures were also measured which showed similar dependences on the annealing time.

2.2. Surface Morphology and Properties

Device performance is related to the morphology of the active layer. From SFM images (Supporting Information Figure S2) the surface rms roughness of the “As-Cast” film was ~5 nm, while the phase image showed features ~10 nm in size. “Pre-Annealing” not only increased the surface roughness to ~7 nm, but also gave rise to aggregates, 50–80 nm in size. “Post-Annealing”, on the other hand, suppressed aggregation at the surface, showing an rms roughness ~5.4 nm, close to the “As-Cast” one. Comparing the SFM images of the “Post-Annealed” samples before and after removing Al, we did not see significant effect of the Al removal by CuCl_2 solution on the surface morphology. We realized the glass transition temperatures (T_g) of the materials is important for understanding the

Table 1. Photovoltaic Characterization Data for PSBTBT:PCBM-based Solar Cell Devices.

Treatment	PCE [%]	V_{oc} [V]	J_{sc} [mA cm^{-2}]	FF [%]
As spun	4.27 ± 0.16	0.59 ± 0.01	14.9 ± 0.4	48.8 ± 1.3
150 °C, 5 sec	4.91 ± 0.14	0.61 ± 0.01	15.3 ± 0.5	52.8 ± 1.3
150 °C, 30 sec	5.03 ± 0.05	0.59 ± 0.01	15.8 ± 0.2	53.6 ± 1.1
150 °C, 1 min	5.17 ± 0.09	0.60 ± 0.01	16.4 ± 0.3	52.8 ± 0.9
150 °C, 5 min	4.61 ± 0.13	0.59 ± 0.01	15.7 ± 0.4	49.4 ± 1.3
150 °C, 10 min	4.19 ± 0.41	0.58 ± 0.01	15.1 ± 0.9	47.3 ± 2.7
150 °C, 20 min	3.73 ± 0.30	0.60 ± 0	14.1 ± 0.4	44.2 ± 2.9

V_{oc} , J_{sc} , FF, PCE represent open-circuit voltage, short-circuit current density, fill factor and power conversion efficiency, respectively. The errors in Table 1 represent the “standard deviation” calculated from the results of more than 20 devices.

morphological changes upon thermal annealing. We have used differential scanning calorimetry to measure the T_g or melting point (T_m) of the pure PSBTBT, but did not see any glass transition or melting or crystallization during several heating and cooling cycles from -100 – 380 °C (PSBTBT decomposes at temperatures above 400 °C based on thermogravimetric analysis).

Water contact angles were used to evaluate the surface properties of the films (Figure 2). The pure PSBTBT film surface is hydrophobic, giving rise to a contact angle of 104.3°, while the surface of the PCBM film is hydrophilic, with a contact angle of 50.6°. The static water contact angle of the “As-Spun” blend film was slightly lower, but very close to that of the pure PSBTBT film, indicating that the surface was richer in PSBTBT than PCBM after spin coating. This is understandable, since PSBTBT has a lower surface energy than PCBM. After “Pre-Annealing” at 150 °C for 1 min, the contact angle of the film surface increased slightly. Increasing the “Pre-Annealing” time to 10 min further increased the contact angle to 103.6° (image not shown), which indicated that “Pre-Annealing” enhanced the surface concentration of PSBTBT. For the “Post-Annealed” sample, after removal of the Al, the contact angle significantly decreased due, more than likely, to the diffusion of PCBM to the interface. This segregation of the PCBM to the cathode/active layer interface is beneficial for device performance, since

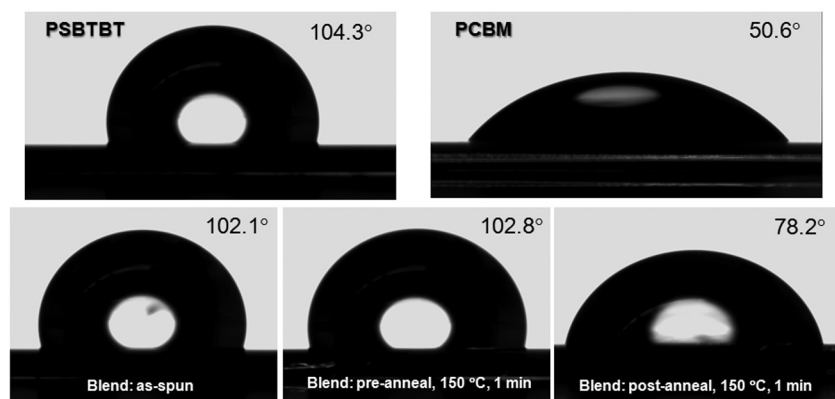


Figure 2. Optical images of static water contact angles on the surfaces of the pure PSBTBT, pure PCBM, and PSBTBT:PCBM blend films under different treatment conditions.

this increases the charge transport to the Al electrode. However, if the film was “Post-Annealed” for longer times, e.g. 10 min, the contact angle increased to 87.8°. This correlates well with the device performance results where short annealing times improved the device performance but longer annealing times degraded the performance. XPS results showed that for the “As-Spun” blend film, PSBTBT was richer at the free surface than at the PEDOT:PSS interface and “Pre-Annealing” increased the concentration of PSBTBT at the free surface (Supporting Information Figure S3).

The molecular orientation at the interfaces is particularly important for charge transport and collection at the electrodes. NEXAFS was used to assess molecular orientation and chemical composition near the surface and the results indicated that there is more “edge-on” orientation than “face-on” structure in the first 10 nm from the surface of the films (see Supporting Information Figure S4). “Pre-Annealing” did not show obvious changes in the electron yields in comparison to those of the “As-Spun” sample, indicating that “Pre-Annealing” did not change the molecular orientation near the surface.

2.3. Depth Profiles

The distribution of the two components in the PSBTBT:PCBM blends as a function of depth in the active layer was studied by DSIMS. To differentiate PSBTBT and PCBM, deuterated PCBM was used in the blend. **Figure 3** shows the DSIMS profiles of the “As-Spun”, “Pre-Annealed”, and “Post-Annealed” blend samples. Within the blend film, the deuterium (D) signal was used as a marker for the PCBM and silicon (Si) for PSBTBT. By the time the ion beam has etched through the layer of PS, a steady-state sputtering rate was achieved. The sharp increase in the D and Si signals marks the surface of the blend film. All the samples showed a uniform distribution of D and Si in the center of the film. However, the “As-Spun” film showed higher concentration of PSBTBT at the surface than in the bulk, and there was a slight depletion of PCBM at the surface. The “Pre-Annealed” sample showed similar behavior to the “As-Spun” film and the enrichment of PSBTBT and depletion of PCBM at the surface were increased upon annealing. However, “Post-Annealing” made the distribution of components in the film more uniform, increasing the concentration of PCBM at the cathode interface, which is in good agreement with the contact angle measurements. In addition, “Post-Annealing” increased the concentration of PSBTBT at the active layer/PEDOT:PSS interface slightly. It should be noted that segregating the donor at the anode and acceptor at the cathode interfaces in OPV devices is beneficial for charge transport and collection, and, as such, “Post-Annealing” led to better device performances.

NR, due to the high contrast of PCBM with PSBTBT and the high spatial resolution, can provide a more detailed description of the distribution of components normal to the surface. **Figure 4A** shows the NR profiles for an “As-Spun” PSBTBT:PCBM film coated on PEDOT:PSS layer surface, along with the film that has been thermally annealed at 150 °C for 1 min. The “As-Spun” and “Pre-Annealed” films have very similar NR profiles. The scattering length density (SLD) profiles, derived from model fits to the data, are shown in the

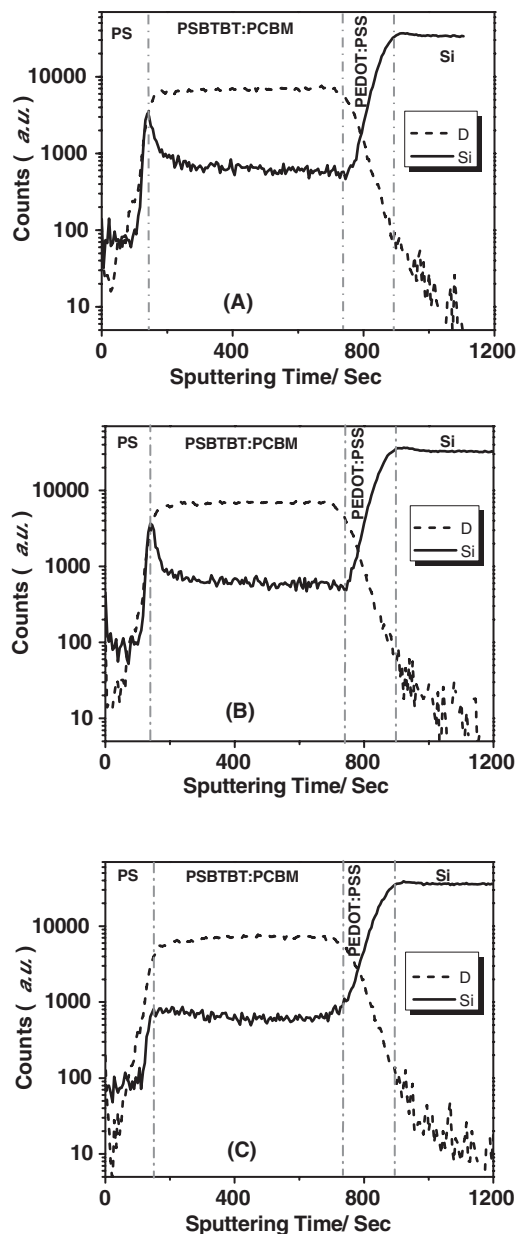


Figure 3. DSIMS profiles for PSBTBT:PCBM blend systems: (A) “As-Spun”, (B) “Pre-Annealed” at 150 °C for 1 min, and (C) “Post-Annealed” at 150 °C for 1 min followed by removal of Al electrodes.

inset of Figure 4A, where the sharp increase at $z = \sim 6$ nm corresponds to the native oxide layer on the Si substrate and at $z = \sim 138$ nm to the air/active layer interface. In the “As-Spun” film the layer located at $z = \sim 7.5\text{--}44$ nm is the PEDOT:PSS film with an SLD of $\sim 1.8 \times 10^{-6} \text{ \AA}^{-2}$, and the thin layer closest to the PEDOT:PSS layer (at $z = \sim 44\text{--}58$ nm) corresponds to the active layer having $\sim 28\%$ PCBM by volume. The bulk of the “As-Spun” active layer had $\sim 57.4\%$ PCBM, which is close to the volume ratio of the two components (53% PCBM and 47% PSBTBT by volume). Near the air/active layer interface, the concentration of PCBM decreased abruptly, showing a PCBM depletion layer

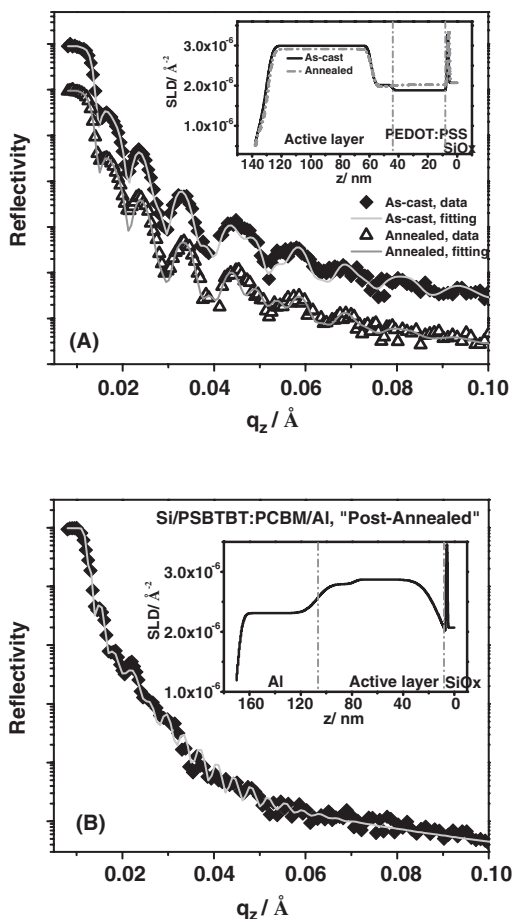


Figure 4. NR profiles of (A) Si/PEDOT:PSS/PSBTBT:PCBM films and (B) Si/PSBTBT:PCBM/Al films. The insets are the corresponding profiles of SLD as a function of z (where $z = 0$ is the Si wafer).

of ~ 8 nm. “Pre-Annealing” slightly increased the thickness of this depletion layer to 9 nm, but did not change the distribution in the bulk. This is quite similar to the DSIMS results. After annealing, the diffuse interface between the active layer and PEDOT:PSS layer with an rms roughness of ~ 7.2 nm, along with the increase in SLD for the PEDOT:PSS layer, indicated that 6% PCBM by volume diffused into the PEDOT:PSS film upon annealing.

The “Post-Annealed” sample, on the other hand, showed markedly different NR and SLD profiles (Figure 4B). In this sample, to simplify the fitting procedure, we did not use the PEDOT:PSS layer, and spin coated the active layer directly on UV-ozone-treated Si substrate, followed by evaporation of an Al electrode on top. The layer located at $z = \sim 10$ – 110 nm corresponded to the active layer, where the two components distributed more uniformly than that in the “As-Spun” and “Pre-Annealed” samples. The drop in the SLD at the substrate suggests a depletion of PCBM (~ 3.8 -nm thick) at the substrate. The layer located at $z = \sim 110$ – 160 nm was ascribed to the aluminum oxide layer. The rough interface between the active layer and the cathode (rms roughness ~ 7.7 nm) indicated the diffusion of Al into the active layer during thermal annealing, which is consistent with the SIMS results on P3HT/PCBM

system.^[26] The interdiffusion between Al and the active layer was also confirmed by high-resolution transmission electron microscopy (HRTEM) image as shown in Supporting Information Figure S5. Comparing the results obtained by DSIMS to those by NR, they are not exactly the same. This is understandable since DSIMS probes a small lateral area (a few square microns) while NR averages over a relatively large area ($3 \text{ cm} \times 4 \text{ cm}$).

2.4. Studies on the Ordering of PSBTBT

GIXD, below and above the critical angle of the active layer but below that of the Si substrate, was used to study the ordering of PSBTBT. Measurements on the “As-Spun”, “Pre-Annealed”, and “Post-Annealed” films were taken at incidence angles of 0.14° and 0.20° , probing the top ~ 10 nm and entire thickness of the blend samples, respectively. A representative 2D GIXD image of the “As-Cast” sample at incidence angle of 0.14° is shown in Supporting Information Figure S6, showing strong scattering in the out-of-plane direction. Figure 5A compares the GIXD profiles for “As-Spun” and “Pre-Annealed” blend

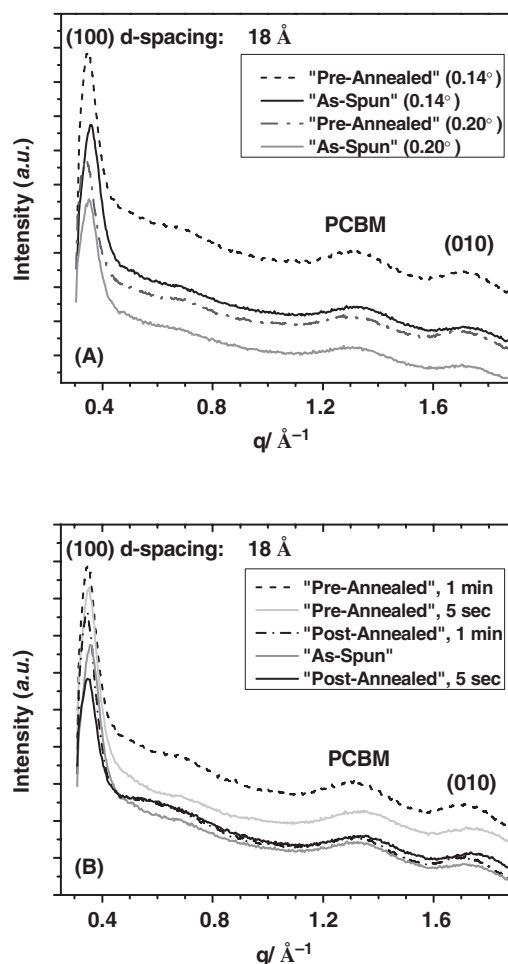


Figure 5. (A) GIXD profiles for PSBTBT:PCBM blend films of “As-Spun” and “Pre-Annealed” at 150°C for 1 min with different incidence angles. (B) GIXD profiles for PSBTBT:PCBM blend films at incidence angle of 0.14° .

films at different incidence angles. The strong diffraction peaks at $q = 0.35 \text{ \AA}^{-1}$ ($d = 17.95 \text{ \AA}$) are attributed to the (100) crystal planes of PSBTBT that are oriented normal to the sample surface, while the (010) crystal planes, corresponding to the π - π stacking of adjacent PSBTBT chains, located at $q = 1.7 \text{ \AA}^{-1}$ ($d = 3.7 \text{ \AA}$), are oriented in-plane. This crystal orientation arises from an “edge-on” orientation of the PSBTBT conjugated planes with the PSBTBT long axes in plane. The peaks at 1.3 \AA^{-1} were attributed to interferences from PCBM. No significant difference in the degree of ordering or orientation was observed at the different incidence angles, but a slight increase in the intensity of the (100) reflection at a 0.14° incidence angle, indicating a higher degree of ordering or orientation of the PSBTBT at the surface.

The effect of different annealing procedures on the ordering of PSBTBT was compared at 0.14° incidence angle in Figure 5B. A well-ordered structure was observed in the “As-Spun” film, which indicated that ordering of the PSBTBT occurred during solvent vapor evaporation. Compared with the “As-Spun” sample, “Post-Annealing” at 150°C for 5 sec decreased the intensity of (100) peak and after 1 min of “Post-Annealing” the intensities of both the (100) and (010) peaks increased. For the “Pre-Annealed” samples, annealing at 150°C for 5 sec and 1 min enhanced the (100) reflection significantly. The spacing of the (100) plane also increased by 0.7 \AA . The results showed that annealing without Al confinement increased the ordering of PSBTBT near the film surface, while annealing under Al confinement did not improve the ordering at the surface significantly. This is in good agreement with the literature studies, in which annealing in the presence of an Al layer on top of the P3HT:PCBM layer restricts the crystal growth and reduces the preferential orientation at the cathode interface, which can be attributed to the Al inter-diffusion.^[31]

The sizes of PSBTBT crystallites in the blend films were calculated using the Scherrer equation,^[40] based on the full width at half maximum of (100) reflections, and a comparison of the different samples at different incidence angles is given in the Supporting Information Table S1. For the “Pre-Annealed” sample, the size of PSBTBT crystallites near the surface increased in comparison to the “As-Spun” film and increased with increasing annealing time. There were no significant changes observed within the bulk of the samples. For the “Post-Annealed” sample, the crystal size at the surface did not increase initially but increased after 1 min, and the size of the crystallites in the entire film increased after “Post-Annealing”. Based on the GIXD results, “Pre-Annealing” improved the ordering of (100) planes of PSBTBT at the surface, while “Post-Annealing” improved the ordering in the bulk. It is worthwhile to note that, with longer annealing times for both the “Pre-Annealed” and “Post-Annealed” samples, the ordering of the PSBTBT in the blends decreased which directly relates to the poorer device performance.

2.5. Small Angle Neutron Scattering (SANS)

SANS provides an ideal means of investigating the size scale of nanoscopic heterogeneities and assessing the uniformity in the distribution and degree of mixing between the two components. Films were spin coated onto silicon wafers that were pre-coated

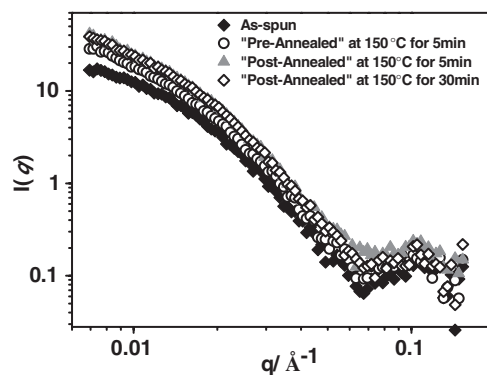


Figure 6. SANS profiles of the PSBTBT:PCBM blend films.

with a layer of PEDOT:PSS. For the “Post-Annealed” samples, annealing was performed after depositing the Al cathode layer and measurements were carried out without removing Al owing to the transparency of Al to neutrons. 10 identical samples were stacked together to provide sufficient sample volume to observe the scattering. A plot of the intensity ($I(q)$) as a function of the scattering vector (q) for the “As-Spun” and annealed solar cell mimics is shown in Figure 6. The SANS profiles are characterized by a minimum at $q = \sim 0.07 \text{ \AA}^{-1}$, followed by a weak maximum at $q = \sim 0.1 \text{ \AA}^{-1}$, corresponding to a $\sim 6.3 \text{ nm}$ spacing characteristic of density correlation and, therefore, phase structure in the plane of the film. Unlike P3HT:PCBM mixtures,^[32] the PSBTBT:PCBM mixtures showed strong scattering even for the “As-Spun” film. From the GIXD results, PSBTBT crystallizes during the spin coating process, and the SANS results show that the ordering of the PSBTBT has forced a segregation of the PCBM to the grain boundaries between ordered PSBTBT domains, forming a multidomained system. In comparison to the “As-Spun” sample, the “Pre-Annealed” sample showed a slight increase in the scattered intensity, indicating a slight purification of the domains; and a slight shift in the maximum to higher q , indicating a reduction in the domain size which is in keeping with a further “demixing” of the PSBTBT and PCBM. The “Post-Annealed” sample, annealed under the same condition, showed an even higher intensity than the “Pre-Annealed” sample and, with further annealing for 30 min, no increase in the scattered intensity was observed.

2.6. Effect of Solvent Evaporation Speed

As mentioned above, the crystallization of PSBTBT and diffusion of PCBM away from the growth front occur during the solvent evaporation process, thus, the speed of the solvent evaporation must impact the ordering of the polymer and the segregation properties of the blend films. The “fast” dried sample was prepared by drop casting a blend solution at 80°C open to the atmosphere, and the “slow” grown sample was kept at room temperature in a sealed jar with a small hole in the lid, allowing the solvent to slowly evaporate. As shown in Figure 7A, the rapidly dried film showed quite weak absorption for PSBTBT and the thermal annealing procedure did not lead to much improvement. While for the slowly dried film,

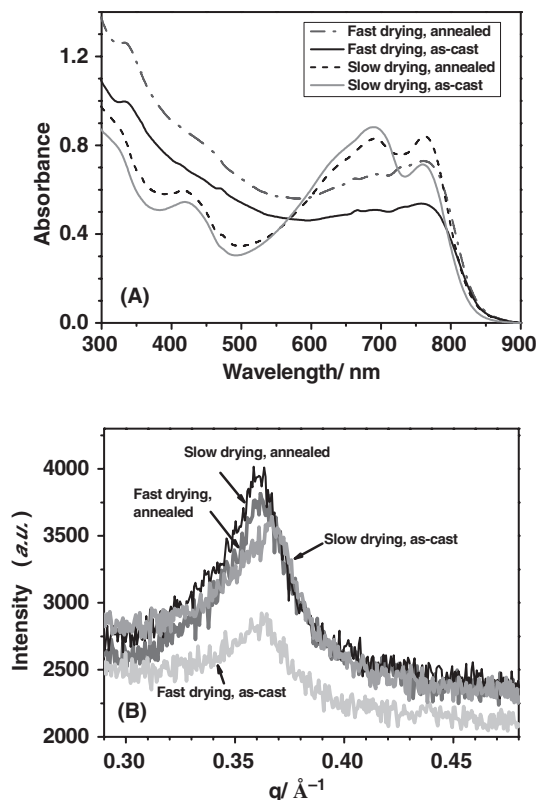


Figure 7. (A) UV-Vis absorption spectra and (B) X-ray diffraction profiles of PSBTBT:PCBM blend (weight ratio 1:2) films prepared by drop casting with fast and slow drying. The “annealed” samples were thermally annealed at 150 °C for 10 min.

the absorption peaks for PSBTBT at 690 and 760 nm were quite strong, and annealing significantly increased the π - π interaction peak at 760 nm.

The ordering of the PSBTBT in the fast and slow evaporation conditions was compared by X-ray diffraction (Figure 7B). The rapidly drying film gave rise to rather weak diffraction peak associated with the (100) crystalline plane and annealing was seen to enhance the ordering. However, for the film prepared under the slow evaporation conditions, the (100) reflection was much stronger and thermal annealing was seen to improve the ordering. It has been reported that by processing with higher boiling point solvent or spin coating at a lower spinning speed to reduce the solvent evaporation rate, more highly ordered materials can be obtained due, primarily, to the enhanced molecular mobility.^[24,41,42] Doctor blading was also used to prepare PSBTBT:PCBM thin films, and the results showed that the sizes of the PSBTBT crystals were \sim 2 nm larger than those of the spin-coated films, which might also be ascribed to the solvent evaporation speed.

2.7. Diffusion of PCBM within PCBM/PSBTBT Bilayer Films

It has been suggested that the increase in performance for P3HT:PCBM BHJ solar cells upon thermal annealing is due to crystallization of disordered P3HT, resulting in the diffusion

of PCBM out of the polymer matrix thereby forming efficient charge transport pathways between the electrodes.^[43] Recently, DSIMS studies on the interdiffusion between PCBM and P3HT in P3HT/PCBM bilayer films revealed that even mild annealing caused significant interdiffusion of both materials, showing that under no conditions do pure amorphous phases exist in BHJ or annealed bilayer devices.^[44,45] In this work, NR was used to study the diffusion of PCBM within the bilayer films of PCBM/PSBTBT. For preparing the bilayer films, PCBM and PSBTBT films were first spin coated onto Si substrates separately, and after drying overnight, the PSBTBT film was then floated onto the surface of water, then retrieve with a PCBM-coated Si substrate, forming a bilayer of PCBM/PSBTBT on the substrate. After removing the water trapped between the two layers in a vacuum oven at room temperature, the samples were annealed at elevated temperatures for different times.

Figure 8A shows the NR profiles for PCBM/PSBTBT bilayer films under different heating treatments. The as-cast film showed well-defined Kiessig fringes, characteristic of the thickness of PCBM layer. As the sample was annealed, the number and amplitude of the fringes decreased significantly, indicating the thinning of the PCBM layer and the roughening of the interface between PCBM and PSBTBT layers.

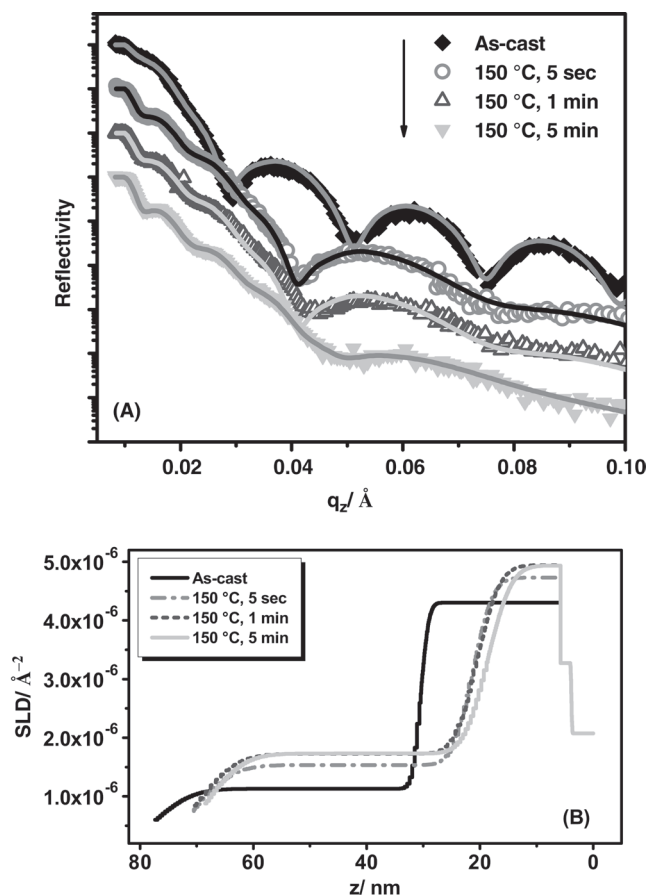


Figure 8. (A) NR profiles for the PCBM/PSBTBT bilayer films (without “Pre-Annealing”) under different annealing conditions. The solid lines indicated the best fits for the reflectivity profiles. (B) The corresponding SLD profiles as a function of z (where $z = 0$ is the Si wafer).

The reflectivity profiles of different samples were fit using a two-layer model, giving rise to the SLD profiles shown in Figure 8B. The sharp interface between the two layers indicates that there was no interdiffusion between PCBM and PSBTBT at room temperature. The diffuse SLD profile at the air/polymer interface is due to the roughness of the PSBTBT film surface during the floating and transfer procedures. After the samples were annealed at 150 °C for only 5 sec, the SLD of the polymer layer increased by 36%, indicating the diffusion of PCBM into the PSBTBT layer and uniform distribution within the PSBTBT layer (see DSIMS results in Figure S7). The SLD of the polymer layer increased further as the sample was annealed for 1 min, and did not show obvious changes after 5 min, suggesting a saturation of PCBM in the PSBTBT. The volume fraction of PCBM in the PSBTBT layer was estimated from the SLD to be 0.19. The slight increase in the SLD of the PCBM film upon annealing at 150 °C can be attributed to a densification of the PCBM. The diffusion behavior of PCBM within the PCBM/PSBTBT bilayers is quite similar to that seen in the PCBM/P3HT system where PCBM was seen to rapidly diffuse into the amorphous regions of P3HT without perturbing the ordering of P3HT.^[32,46]

3. Conclusions

In this work, we used a broad range of techniques to investigate the morphologies of PSBTBT:PCBM blend films to mimic actual devices. Similar to results on P3HT, an enrichment of PSBTBT and depletion of PCBM at the free surface is found in the “As-Spun” PSBTBT:PCBM blend films. Thermal annealing in the absence of Al cathodes increased this segregation, while annealing after the deposition of the Al cathode led to an increase in the concentration of PCBM at this interface. This segregation of components to the interface directly correlated with the device performance. GIXD and SANS studies showed that the ordering of the PSBTBT and segregation of PCBM occurred during solution casting, and a “Post-Annealing” increased the ordering of PSBTBT and enhanced the segregation of PCBM, forming domains ~10-nm in size, which also contributed to improving device performance. Studies on PCBM diffusion within PCBM/PSBTBT bilayer films by NR provided evidence that PCBM can only diffuse along the PSBTBT crystalline grains and aggregated or dispersed within the disordered regions of the polymer.

4. Experimental Section

Poly[(4,4'-bis(2-ethylhexyl)dithieno[3,2-b:2',3'-d]silole)-2,6-diyl-alt-(4,7-bis(2-thienyl)-2,1,3-benzothiadiazole)-5,5'-diyl] (PSBTBT) and phenyl-C61-butyric acid methyl ester (PCBM) were provided by Konarka Inc.^[47] Both PSBTBT and PCBM were dissolved in 1,2-dichlorobenzene (*o*-DCB, 99%, Sigma-Aldrich)^[47] in a 1:1.5 (12 mg mL⁻¹: 18 mg mL⁻¹) wt ratio. The solution was stirred at 80 °C for 2 days to make the two components completely dissolved followed by filtering with 0.45 μm syringe filters. The hot solution was then spin coated onto indium tin oxide (ITO)/glass substrates pre-coated with a 35-nm-thick layer of PEDOT:PSS [poly(ethylenedioxythiophene):polystyrene sulfonate, CLEVIOS™ PH 500].^[47] The thickness of the active layer was ~104 nm, as determined by an Alpha-step IQ Surface Profiler (KLA-Tencor Corporation).^[47] A 100 nm thick Al electrode was then thermally evaporated onto the

surface of the active layer under high vacuum (1.5×10^{-6} Torr) using a thermal evaporator. The active area of the device was ~0.06 cm² for all the devices measured in this work. The devices were thermally annealed before or after deposition of the cathode, termed “Pre-Annealing” or “Post-Annealing”, respectively. Device characterization was performed in an N₂ atmosphere under simulated AM1.5G irradiation (100 mW cm⁻²) using a xenon lamp-based solar simulator (Newport 91160 300-W Solar Simulator).^[47]

For structural characterization, the blend films were prepared on Si substrates pre-coated with a PEDOT:PSS layer, denoted as Si/PEDOT:PSS/PSBTBT:PCBM. For preparation of the “Post-Annealed” samples, the Al electrodes were removed with CuCl₂ solution (0.2 M) after thermal annealing. The surface was then repeatedly rinsed with ethanol and distilled water. For the SANS and NR measurements, the Al layer on the “Post-Annealed” samples was not removed.

GIXD measurements were performed at the Advanced Light Source, Lawrence Berkeley National Laboratory, Berkeley, CA. SANS measurements were performed at General-Purpose Small-Angle Neutron Scattering Diffractometer CG-2 beam line at High Flux Isotope Reactor (HFIR) at the Oak Ridge National Laboratory, Oak Ridge, TN. NR experiments were performed at Magnetism Reflectometer BL-4A beam line at Spallation Neutron Source (SNS) in Oak Ridge National Laboratory, Oak Ridge, TN.

DSIMS measurements were performed on the Physical Electronics 6650 Quadrupole Secondary Ion Mass Spectrometry System at the University of California, Santa Barbara. To establish a constant sputtering rate, a 30-nm-thick film of polystyrene (PS) was placed on the top of the samples.^[48] The film was prepared by spin coating toluene solutions of PS onto a Si substrate. The thin PS film was then removed from the substrate by floating onto water and picked up on top of the samples. The samples were dried at room temperature under vacuum to remove residual water.

UV-Vis absorption spectra were recorded with a UV-3600 UV-VIS-NIR Spectrophotometer from Shimadzu Corporation.^[47] The contact angle measurements were performed by the static sessile drop method on an OCA20 Interfacial Tension Measuring Device (Future Digital Scientific Co.).^[47]

Supporting Information

Supporting Information is available from the Wiley Online Library or from the author.

Acknowledgements

This work is funded by the US Department of Energy Office of Basic Energy Science (TPR) and the DOE-supported Energy Frontier Research Center on Polymer-Based Materials for Harvesting Solar Energy (HL, TPR) at the University of Massachusetts-Amherst. We are grateful to Konarka Inc. for providing materials and financial support (HL) during the course of these studies. HL is also grateful to Dr. Volodymyr Duzhko (University of Massachusetts-Amherst) for assistance with the UPS measurements, Dr. Dongguang Wei (Carl Zeiss NTS LLC) for the HRTEM measurements, and Dr. Tom Mates (UCSB) for the DSIMS measurements. Support of the Materials Research Science and Engineering Center and its Materials Science Facilities Network program for facilitating the DSIMS measurements are acknowledged. Use of the Advanced Light Source at Berkeley National Laboratory and High Flux Isotope Reactor and Spallation Neutron Source at the Oak Ridge National Laboratory, both supported by the DOE, Office of Science, Office of Basic Energy Science, are also acknowledged.

Received: March 12, 2011

Revised: June 17, 2011

Published online:

- [1] R. Giridharagopal, D. S. Ginger, *J. Phys. Chem. Lett.* **2010**, *1*, 1160.
- [2] H. Hoppe, N. S. Sariciftci, *J. Mater. Chem.* **2006**, *16*, 45.
- [3] X. Yang, J. Loos, *Macromolecules* **2007**, *40*, 1353.
- [4] S. van Bavel, S. Veenstra, J. Loos, *Macromol. Rapid Commun.* **2010**, *31*, 1835.
- [5] S. S. Lee, Y. L. Loo, in *Annual Review of Chemical and Biomolecular Engineering, Vol 1*, Annual Reviews, Palo Alto **2010**, 59.
- [6] J. Peet, A. J. Heeger, G. C. Bazan, *Accounts Chem. Res.* **2009**, *42*, 1700.
- [7] F. Padinger, R. S. Rittberger, N. S. Sariciftci, *Adv. Funct. Mater.* **2003**, *13*, 85.
- [8] S. Nam, M. Shin, H. Kim, Y. Kim, *Nanoscale* **2010**, *2*, 2384.
- [9] E. Verploegen, R. Mondal, C. J. Bettinger, S. Sok, M. F. Toney, Z. A. Bao, *Adv. Funct. Mater.* **2010**, *20*, 3519.
- [10] B. F. Xue, B. Vaughan, C. H. Poh, K. B. Burke, L. Thomsen, A. Stapleton, X. J. Zhou, G. W. Bryant, W. Belcher, P. C. Dastoor, *J. Phys. Chem. C* **2010**, *114*, 15797.
- [11] O. Douheret, L. Lutsen, A. Swinnen, M. Breselge, K. Vandewal, L. Goris, J. Manca, *Appl. Phys. Lett.* **2006**, *89*, 032107.
- [12] M. Dante, J. Peet, T. Q. Nguyen, *J. Phys. Chem. C* **2008**, *112*, 7241.
- [13] E. J. Spadafora, R. Demadrille, B. Ratier, B. Grevin, *Nano Lett.* **2010**, *10*, 3337.
- [14] D. S. Germack, C. K. Chan, B. H. Hamadani, L. J. Richter, D. A. Fischer, D. J. Gundlach, D. M. DeLongchamp, *Appl. Phys. Lett.* **2009**, *94*, 233303.
- [15] D. S. Germack, C. K. Chan, R. J. Kline, D. A. Fischer, D. J. Gundlach, M. F. Toney, L. J. Richter, D. M. DeLongchamp, *Macromolecules* **2010**, *43*, 3828.
- [16] M. Y. Chiu, U. S. Jeng, M. S. Su, K. H. Wei, *Macromolecules* **2010**, *43*, 428.
- [17] T. Erb, U. Zhokhavets, G. Gobsch, S. Raleva, B. Stuhn, P. Schilinsky, C. Waldauf, C. J. Brabec, *Adv. Funct. Mater.* **2005**, *15*, 1193.
- [18] M. Shin, H. Kim, J. Park, S. Nam, K. Heo, M. Ree, C. S. Ha, Y. Kim, *Adv. Funct. Mater.* **2010**, *20*, 748.
- [19] C. H. Woo, B. C. Thompson, B. J. Kim, M. F. Toney, J. M. J. Frechet, *J. Am. Chem. Soc.* **2008**, *130*, 16324.
- [20] M. Y. Chiu, U. S. Jeng, C. H. Su, K. S. Liang, K. H. Wei, *Adv. Mater.* **2008**, *20*, 2573.
- [21] S. Swaraj, C. Wang, H. P. Yan, B. Watts, L. N. Jan, C. R. McNeill, H. Ade, *Nano Lett.* **2010**, *10*, 2863.
- [22] B. Watts, W. J. Belcher, L. Thomsen, H. Ade, P. C. Dastoor, *Macromolecules* **2009**, *42*, 8392.
- [23] A. C. Arias, N. Corcoran, M. Banach, R. H. Friend, J. D. MacKenzie, W. T. S. Huck, *Appl. Phys. Lett.* **2002**, *80*, 1695.
- [24] M. Campoy-Quiles, T. Ferenczi, T. Agostinelli, P. G. Etchegoin, Y. Kim, T. D. Anthopoulos, P. N. Stavrinou, D. D. C. Bradley, J. Nelson, *Nat. Mater.* **2008**, *7*, 158.
- [25] Z. Xu, L. M. Chen, G. W. Yang, C. H. Huang, J. H. Hou, Y. Wu, G. Li, C. S. Hsu, Y. Yang, *Adv. Funct. Mater.* **2009**, *19*, 1227.
- [26] J. N. Audinot, P. Leveque, R. Bechara, N. Leclerc, J. Guillot, H. N. Migeon, G. Hadziioannou, T. Heiser, *Surf. Interface Anal.* **2010**, *42*, 1010.
- [27] J. W. Kiel, B. J. Kirby, C. F. Majkrzak, B. B. Maranville, M. E. Mackay, *Soft Matter* **2010**, *6*, 641.
- [28] A. J. Parnell, A. D. F. Dunbar, A. J. Pearson, P. A. Staniec, A. J. C. Dennison, H. Hamamatsu, M. W. A. Skoda, D. G. Lidzey, R. A. L. Jones, *Adv. Mater.* **2010**, *22*, 2444.
- [29] J. W. Kiel, M. E. Mackay, B. J. Kirby, B. B. Maranville, C. F. Majkrzak, *J. Chem. Phys.* **2010**, *133*, 074902.
- [30] H. J. Kim, H. H. Lee, J. J. Kim, *Macromol. Rapid Commun.* **2009**, *30*, 1269.
- [31] H. J. Kim, J. H. Park, H. H. Lee, D. R. Lee, J. J. Kim, *Org. Electron.* **2009**, *10*, 1505.
- [32] D. Chen, A. Nakahara, D. Wei, D. Nordlund, T. P. Russell, *Nano Lett.* **2011**, *11*, 561.
- [33] A. Orimo, K. Masuda, S. Honda, H. Benten, S. Ito, H. Ohkita, H. Tsuji, *Appl. Phys. Lett.* **2010**, *96*, 043305.
- [34] J. H. Hou, H. Y. Chen, S. Q. Zhang, G. Li, Y. Yang, *J. Am. Chem. Soc.* **2008**, *130*, 16144.
- [35] M. C. Scharber, M. Koppe, J. Gao, F. Cordella, M. A. Loi, P. Denk, M. Morana, H. J. Egelhaaf, K. Forberich, G. Dennler, R. Gaudiana, D. Waller, Z. G. Zhu, X. B. Shi, C. J. Brabec, *Adv. Mater.* **2010**, *22*, 367.
- [36] M. Morana, H. Azimi, G. Dennler, H. J. Egelhaaf, M. Scharber, K. Forberich, J. Hauch, R. Gaudiana, D. Waller, Z. H. Zhu, K. Hingerl, S. S. van Bavel, J. Loos, C. J. Brabec, *Adv. Funct. Mater.* **2010**, *20*, 1180.
- [37] H. Y. Chen, J. H. Hou, A. E. Hayden, H. Yang, K. N. Houk, Y. Yang, *Adv. Mater.* **2010**, *22*, 371.
- [38] G. Dennler, M. C. Scharber, C. J. Brabec, *Adv. Mater.* **2009**, *21*, 1323.
- [39] R. C. Coffin, J. Peet, J. Rogers, G. C. Bazan, *Nat. Chem.* **2009**, *1*, 657.
- [40] L. E. Alexander, *X-ray Diffraction Methods in Polymer Science*, John Wiley & Sons, Inc, New York **1969**.
- [41] J. F. Chang, B. Q. Sun, D. W. Breiby, M. M. Nielsen, T. I. Solling, M. Giles, I. McCulloch, H. Sirringhaus, *Chem. Mat.* **2004**, *16*, 4772.
- [42] G. Li, V. Shrotriya, J. S. Huang, Y. Yao, T. Moriarty, K. Emery, Y. Yang, *Nat. Mater.* **2005**, *4*, 864.
- [43] J. Jo, S. S. Kim, S. I. Na, B. K. Yu, D. Y. Kim, *Adv. Funct. Mater.* **2009**, *19*, 866.
- [44] B. A. Collins, E. Gann, L. Guignard, X. He, C. R. McNeill, H. Ade, *J. Phys. Chem. Lett.* **2010**, *1*, 3160.
- [45] N. D. Treat, M. A. Brady, G. Smith, M. F. Toney, E. J. Kramer, C. J. Hawker, M. L. Chabinyc, *Adv. Energy Mater.* **2011**, *1*, 82.
- [46] D. Chen, F. Liu, C. Wang, A. Nakahara, T. P. Russell, *Nano Lett.* **2011**, *11*, 2071.
- [47] Certain equipment, instruments or materials are identified in this paper in order to adequately specify the experimental details. Such identification does not imply recommendation by the NIST, nor does it imply the materials are necessarily the best available for the purpose.
- [48] G. Coulon, T. P. Russell, V. R. Deline, P. F. Green, *Macromolecules* **1989**, *22*, 2581.